Desalination and Water Treatment
www.deswater.com

doi: 10.5004/dwt.2019.24503

166 (2019) 344–352
October

Performance and mechanism of Cr(VI) removal by resin-supported nanoscale zero-valent iron (nZVI): role of nZVI distribution

Yuan Wang[a], Yaqin Song[a], Chenfei Shi[b], Jingge Shang[a], Jianqiu Chen[a,*], Qiong Du[a,*]

[a]*School of Engineering, China Pharmaceutical University, Nanjing, 211198, China, Tel. (025) 8618 5190; emails: cjqer@163.com (J. Chen), duqiong116@163.com (Q. Du), wangyuan181151@163.com (Y. Wang), 1002779434@qq.com (Y. Song), shangjingge@163.com (J. Shang)*
[b]*School of Environment, Nanjing Normal University, Nanjing, 210023, China, Tel. (025) 8618 5190; email: schenfei@njnu.edu.cn*

Received 7 January 2019; Accepted 5 June 2019

ABSTRACT

Four composite resins with different nanoscale zero-valent iron (nZVI) distributions were used to remove hexavalent chromium (Cr(VI)) from water. The effects of nZVI distributions on the performances and mechanisms of the composite resins were investigated during the Cr(VI) removal process. The stability experiments showed that the hybrids with a more uniform nZVI distribution than others were more favorable for inhibiting nZVI dissolution into iron ions under acidic pH (1.5–3.5), and that hybrids with different nZVI distributions exhibited no significant differences in Cr(VI) removal under the influences of aging and solution pH. Results of the reactivity experiments showed that the Cr(VI) removal efficiency decreased with increasing initial Cr(VI) concentration, and that 72.09%–97.18% of 100 mg/L Cr(VI) could be removed from aqueous solutions by four composite resins with different nZVI distributions. The presence of phosphate, silicate, and nitrate inhibited Cr(VI) removal; further, the hybrids with a more uniform nZVI distribution than others exhibited a better removal selectivity. The adsorption kinetics data agreed well with those from the pseudo-second-order model ($R^2 \geq 0.9710$). The reactivity experiments combined with X-ray photoelectron spectroscopy showed that the composite resin with a peripheral nZVI distribution has a strong reduction ability and high removal performance. With increasing uniformity in the nZVI distribution, the reduction performance weakened and the adsorption performance enhanced during Cr(VI) removal. The findings of this study demonstrate the importance of nZVI distribution on Cr(VI) reduction and immobilization when the nZVI nanocomposite is applied to treat Cr(VI) contaminants. The results will help to optimize the design and fabrication of nZVI nanocomposites of improved reactivity for environmental decontamination.

Keywords: Performance; Mechanisms; Cr(VI) removal; Nanoscale zero-valent iron; Distributions

1. Introduction

Chromium is one of the most toxic heavy metals in water; it causes damage to organs such as the liver and kidneys, and may induce genetic mutations in humans [1,2]. Chromium mainly exists in trivalent (Cr(III)) and hexavalent (Cr(VI)) oxidation states in natural water [3]. Cr(VI) is the most toxic and mobile form owing to its high oxidizing ability and solubility in water. In contrast, Cr(III) is a relatively insoluble, immobile, and less harmful species [4,5]. Therefore, most remediation technologies aim to reduce Cr(VI) to the less dangerous Cr(III) species [6]. In recent

* Corresponding authors.

years, zero-valent iron (ZVI) has been proven to be effective for the reduction of many kinds of pollutants (e.g., Cr(VI), As(V), Se(VI), and nitrates) in groundwater, wastewater, and laboratory studies via reduction, adsorption, and co-precipitation [7]. Particularly, nanoscale zero-valent iron (nZVI) has attracted increasing attention because of its high activity and wide availability [8]. However, nZVI usually occurs as fine powders, and hence, may require a complicated and difficult separation process in practical applications and cannot be applied in fixed-bed operations [9]. Moreover, nZVI particles are susceptible to strong aggregation into microscale or larger scale particles, resulting in a decrease in the specific surface area and intrinsic reactivity, which poses potential limitations to its application in environmental remediation [10].

To solve these problems, researchers have attempted the loading of nZVI onto supports such as bentonite, mesoporous silica, activated carbon, resins, and biochar [11–15]. In recent years, nZVI supported on cation exchange resins has been efficiently utilized for the removal of Cr(VI) [16–18]. However, Cr(VI) exists in the anionic form and cannot be ion-exchanged in the cation resin. Therefore, a cation exchange resin only serves as a carrier and dispersant in Cr(VI) removal. In a previous work, a strongly basic macroporous styrene-type anion exchange resin (D201) was employed to fabricate a nanocomposite (D201-nZVI) by anion exchange and chemical reduction in situ [19]. Owing to the non-diffusible positive charge provided by the quaternary ammonium groups ($-N^+(CH_3)_3$) present on the host backbone, an anionic pollutant could be favorably preconcentrated into the pores prior to their subsequent removal by the embedded nZVI nanoparticles. Considering that Cr(VI) exists in the anionic form ($HCrO_4^-$, CrO_4^{2-}) over a wide range of pH, it can be reasonably expected that the resultant nanocomposite (D201-nZVI) would be promising for Cr(VI) removal by combining the advantages of the support material D201 and nZVI particles. A synergistic process of Cr(VI) removal involving anion exchange, adsorption, and chemical reduction could be anticipated by employing the resultant nanocomposite (D201-nZVI). However, the performance and mechanism of Cr(VI) removal by the proposed material was not clear. Particularly, the relationship between the spatial distribution of nZVI in the nanocomposite and the performance and mechanism of Cr(VI) removal has never been reported.

The structure–activity relationship of the composite has been studied on nitrate reduction and photocatalytic properties in published papers [20,21]. Therein, the activity difference was proved to be related to the distribution of the active ingredients. Despite the different roles of the supported nZVI, bimetallic Pd-Cu, and CdS in pollutant removal, we suggested that supported nZVI with different distributions might exhibit different performances in terms of reactivity, chemical stability, and removal mechanism. The main objective of this study is to investigate the role of nZVI spatial distribution in the performance and mechanism of resin-supported nZVI in Cr(VI) removal. The chemical stability and reactivity of the nanocomposite were studied through batch tests, and X-ray photoelectron spectroscopy (XPS) analysis was performed to elucidate the possible mechanism of Cr(VI) removal.

2. Materials and methods

2.1. Materials

The support, the D201 macroporous anionic exchanger, which is a polystyrene-divinylbenzene polymer matrix with tetraamine functional groups, was kindly supplied by Zhejiang Zhengguang Industrial Co. Ltd., China. Prior to use, it was rinsed sequentially with NaOH (5 wt%), HCl (5 wt%), and distilled water until a neutral pH was reached, and dried at 40°C for 24 h. All chemicals used in this work were of analytical grade or higher and used as received without further purification. A stock solution of Cr(VI) was prepared by dissolving potassium dichromate ($K_2Cr_2O_7$) in ultrapure water. Cr(VI) working solutions were freshly prepared by diluting the stock solution with ultrapure water.

2.2. Synthesis of nanocomposite with different nZVI distributions

The resin-supported nZVI (D201-nZVI) was prepared using a borohydride reduction method described in our previous report [22]. In brief, D201 (1.0 g) was added to 100 mL of $FeCl_4^-$ solution in a constant-temperature water bath at 25°C for 4 h, and washed with anhydrous ethanol several times. The preloaded $FeCl_4^-$ ions of the resin could be reduced into nZVI with different distributions using KBH_4 solutions with mass concentrations of 0.9%, 1.8%, 3.6%, and 7.2%, and the products were denoted as D1, D2, D3, and D4, respectively [22]. The iron contents of D1, D2, D3, and D4 were approximately equal (10.30%, 10.56%, 10.11%, and 10.83%, respectively). ZVI immobilized with D201 occurs in the form of nanoscale particles, as confirmed by XRD and XPS in our previous work [23].

2.3. Stability experiments

The iron release experiment was performed to investigate the iron releases of D1, D2, D3, and D4 under acidic conditions. In the experiment, 0.1 g of the sample (D1, D2, D3, and D4) was weighed into 100 mL of an aqueous solution (pH adjusted to 1.5, 2.0, 3.0, and 3.5, respectively), and the Fe concentrations and solution pH at equilibrium were determined.

The effect of solution pH values on Cr(VI) removal was investigated by weighing 0.1 g D1, D2, D3, and D4 into 150 mg/L Cr(VI) solution, respectively, and varying the pH (3.0–11.0). The different solution pHs were well adjusted by adding 1 mol/L NaOH or HCl.

D1, D2, D3, and D4 were aged by charging 0.1 g of composite resins into 150 mL conical flasks containing 100 mL of deionized water. The conical flasks were shaken for 48 h or 72 h at 25°C and 160 rpm. The aging effect on Cr(VI) removal was investigated by using 0.1 g of the aged composite resin to remove Cr(VI) from 500 mL of 35 mg/L Cr(VI) aqueous solutions. The experimental conditions of the above experiments were: shaking at 25°C and 160 rpm for 24 h.

2.4. Reactivity experiments

The effect of the initial concentration was determined by setting the initial concentration of Cr(VI) as 30, 100, 200,

or 300 mg/L, respectively. The effect of coexisting ions was determined by adding 100 mmol/L of $H_2PO_4^-$, NO_3^-, or SiO_3^{2-} to the solution (100 mL). Kinetic tests were carried out in a 500 mL solution containing 30 mg/L Cr(VI) ions and 0.2 g/L of composite resins. At regular time intervals, the solutions were sampled and measured.

2.5. Characterization and analysis methods

The surface characteristics and elemental distribution of the composite resins were measured by scanning electron microscopy–energy-dispersive X-ray spectroscopy (SEM–EDS, Hitachi S-4800, Hitachi, Japan). The composite resins after the reaction were analyzed by XPS (ESCALAB 250XI, Thermo Scientific, United States), and XPS data processing and peak fitting were performed using the nonlinear least squares fitting procedure (XPS Peak software V4.1).

The pH value was determined with a pH meter (PB-10, Rex, China). The concentration of iron was measured with o-phenanthroline spectrophotometry. The concentrations of aqueous Cr(VI) were determined with the diphenylcarbazide method using a UV–visible spectrophotometer (UV-754, Jinghua, China) at 540 nm wavelength. The minimum detectable concentration by this method was 0.004 mg/L. The relative standard deviation of the method was 2.1%, the relative error was 0.13% [24]. The standard curve of Cr(VI) was obtained by experimental method and the R^2 of the standard curve was 0.9991.

3. Results and discussion

3.1. Structure characteristics of composite resins

The distribution of Fe in the composite resin (D1–D4) as determined by SEM–EDS analysis is shown in Fig. 1. The Fe in D1 is present at the periphery of the resin and forms a ring around the resin. With an increase in the concentration of KBH_4, Fe is gradually formed in the interior of the resin, and is uniformly distributed throughout the resin up to a KBH_4 concentration of 7.2%. That is, the Fe distribution in D1–D4 changed from peripheral ring-like region to uniform distribution in the entire matrix of the supporting resin with increasing concentration of KBH_4. The structure of the four composite resins could also be verified by the relationship between the strength of iron and the diameter distance of iron in the resin in SEM–EDS linear scanning (Fig. 1b). This is because the nZVI distribution was the result of a balance between two reactions: hydrolyzation of $FeCl_4^-$ into Fe^{3+} and reduction of Fe(III) species by KBH_4 [19].

3.2. Stability of the composite resin

3.2.1. pH-dependent stability of the four hybrids

The pH-dependent iron release from the nanocomposites (D1–D4) is illustrated in Fig. 2a. It can be seen that the Fe dissolution ratio in the composite resin reached 70.87% at pH = 1.5. The Fe dissolution ratio decreased as the pH increased and was 0.001% at pH = 3.5. When the pH was 1.5, the Fe dissolution of D1 to D4 was 85.15%, 79.36%, 79.28%, and 70.87%, and at pH 2.0, it was 80.71%, 66.61%, 65.67%, and 50.90%, respectively. A comparison of the four nanocomposites showed that the Fe dissolution ratio was relatively higher in the sample with a peripheral distribution of Fe, that is, D1. The results indicated that the peripheral nZVI had little protection from the resin skeleton as it was mainly distributed on the periphery of the support, which led to its easy contact with H^+ in a strong acidic solution. Conversely, the Fe dissolution ratio decreased as the nZVI distribution into the composite resins became closer to the center of the composite resin. This is because the quaternary amine groups of the resin could hinder the contact between the internal nZVI and H^+ of the solution. All the dissolution rates reduced to 1.5% at pH 3 and were less than 0.001% at pH 3.5. To avoid the effect of iron leaching on the removal of Cr(VI), the pH of the solution in the following experiment was maintained at ≥3.0.

The effect of pH (3.0, 5.0, 7.0, and 11.0) on the removal of Cr(VI) from aqueous solutions is depicted in Fig. 2b. The composite resins exhibited a better adsorption for the anions, and Cr(VI) was in the anionic form ($HCrO_4^-$,CrO_4^{2-}) at pH > 3. Thus, the removal rate should increase with increasing pH. However, the removal rates of the four composite

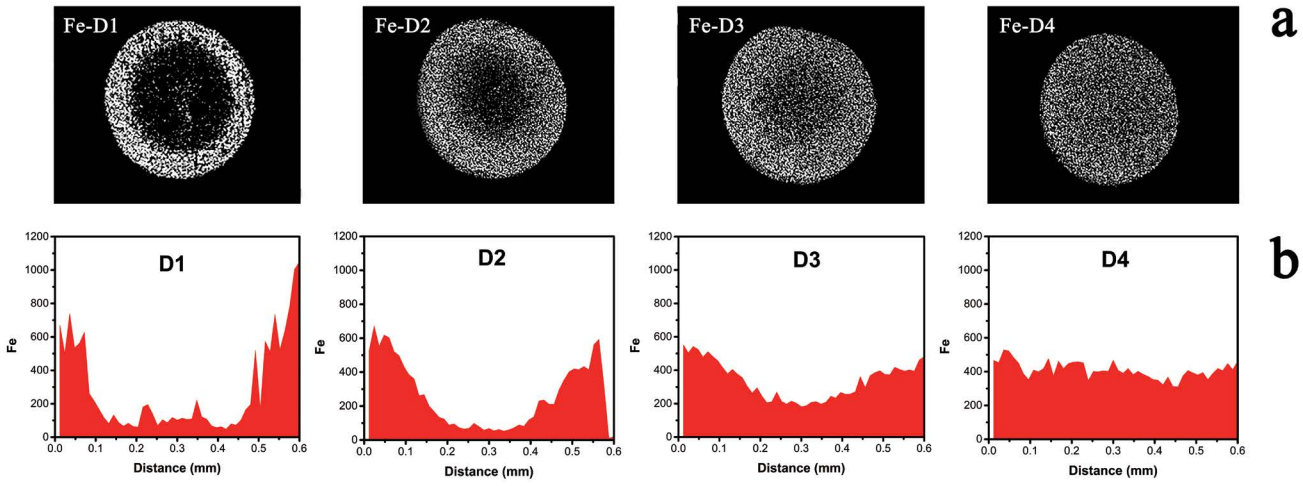

Fig. 1. Elemental Fe distribution in the cross section of D1–D4: (a) SEM-EDS surface scanning and (b) SEM-EDS linear scanning.

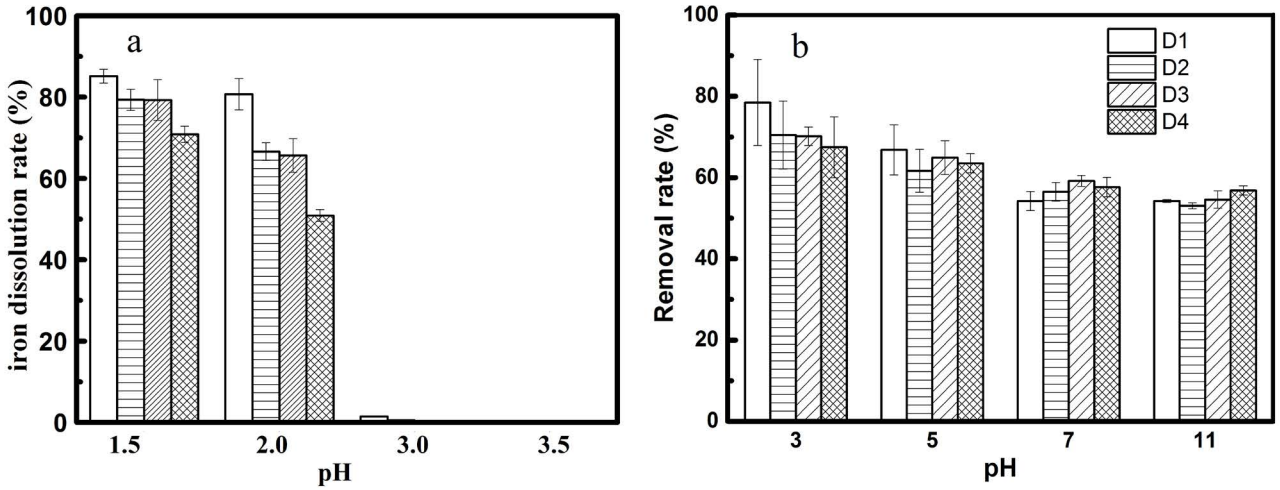

Fig. 2. Effect of initial solution pH on (a) Fe release from D1-D4 and (b) Cr(VI) removal by D1-D4.

resins slightly decreased when the pH was increased from 3.0 to 11.0. A plausible reason is that the increase in OH^- concentration in the solution resulted in a competition for the adsorption site of the resin with increasing pH, which led to a slight decrease in the removal rate. In addition, $HCrO_4^-$, gradually converted into CrO_4^{2-} at pH ≥ 6.5, indicates that the composite resins significantly adsorbed $HCrO_4^-$. Moreover, the isoelectric point (IEP) of the nZVI was approximately 8.1 [25,26]; thus, the surface of the nZVI was negatively charged when the solution pH was higher than the IEP and had a lower affinity toward CrO_4^{2-}, which further decreased the removal rate. The difference in the removal rate of the four composite resins was less than 11% at pH = 3 and less than 5% at pH > 3. Nevertheless, the removal rate was about 60% for all composite resins. There was no significant difference in the removal rates under different pH values for different nZVI distributions.

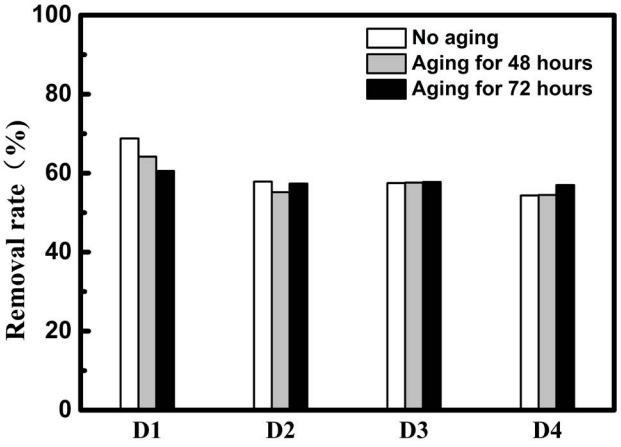

Fig. 3. Effect of aging on Cr(VI) removal.

3.2.2. Aging-dependent stability of the four hybrids

The composite resins were aged in water for a short time and then used to remove Cr(VI) to evaluate the effect of aging on Cr(VI) removal. Fig. 3 shows that there is almost no significant change in the removal rate of the fresh composite resins (D2, D3, and D4) compared with the 72 h aged composite resins; the removal rate of D1 decreased slightly by less than 10%. The decrease might be due to the easy oxidizability of the peripheral nZVI of D1, which affects its activity. These findings suggest that the differences in elemental Fe distribution would affect the iron release of D1–D4, but had little effect on the influences of solution pH and aging on Cr(VI) removal under the above experimental conditions.

3.3. Reactivity of composite resin

3.3.1. Cr(VI) Removal by D201 and D201-nZVI

The removal of Cr(VI) was compared among five materials (D201, D1, D2, D3, and D4). As shown in Fig. 4, the removal percentages of Cr(VI) were all above 99.6%. The presence of silicate at 100 mM significantly inhibited Cr(VI) removal (only 16.87%) by the host anion exchanger D201, which could be attributed to the severe competition from the coexisting silicate for ion exchange sites. For the composite resins D1–D4, 22.44%–41.67% removal of Cr(VI) was observed, because silicate could form inner-sphere complexes with iron (oxy)hydroxides and inhibit Cr(VI) adsorption on ZVI surface. Compared with the host anion exchanger D201, the composite resins, especially the hybrids with more uniform nZVI distribution, exhibited a better removal selectivity. In addition, D201 only had an enrichment effect on the treatment of Cr(VI), and could not reduce Cr(VI) to Cr (III), which is less toxic. This proved the challenge of the ion-exchange strategy in the removal of Cr(VI) from natural water.

3.3.2. Effect of initial concentration on Cr(VI) removal

The effect of initial Cr(VI) concentration (30–300 mg/L) on the Cr(VI) removal rate of the composite resins is displayed in Fig. 5. At a lower concentration (30 mg/L), the removal of Cr(VI) was higher than 97.5%. However, when Cr(VI) was concentrated up to 300 mg/L, the removal of Cr(VI) decreased to 51.3%. The Cr(VI) removal rate

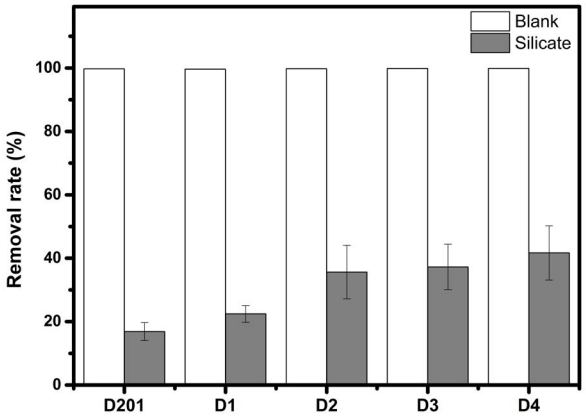

Fig. 4. Cr(VI) removal by D201 and four composite resins with/without silicate.

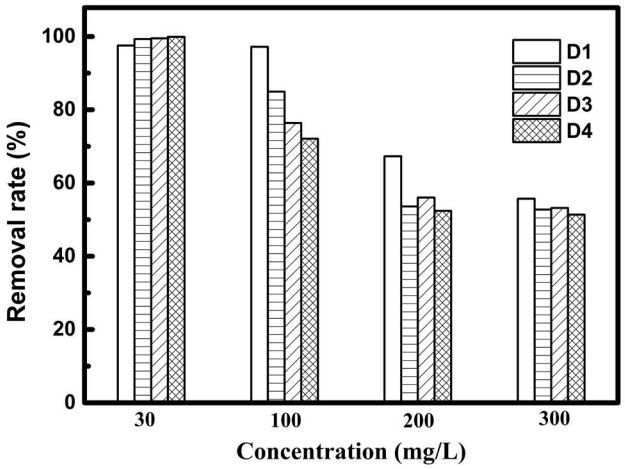

Fig. 5. Effect of initial Cr(VI) concentration on Cr(VI) removal by D1-D4.

decreased with increasing initial Cr(VI) concentration, possibly because the added composite resins were not enough to completely react with Cr(VI) with increasing initial Cr(VI) concentration. Compared with previously published data on the use of iron nanocomposites for chromium removal [16], the composite resin D201-nZVI not only had the ability of reducing Cr(VI) but also had the ability of adsorbing Cr(VI), which has a better removal effect on Cr(VI). At the concentration of 30 mg/L, Cr(VI), Q was approximately 1.03 mg/g as reported in previously published data for the nZVI composite resin based on cationic exchange [16], but was greater than 29.25 mg/g in the present study for the nZVI composite resin based on anion exchange resin (D201). No significant difference was observed among D1, D2, D3, and D4 at 30 mg/L Cr(VI) concentration. However, when the Cr(VI) concentration increased to 100 mg/L, the Cr(VI) removal efficiency decreased in the order of D1 > D2 > D3 > D4, indicating that the removal ability of D1 was higher than that of the others. A further increase in Cr(VI) concentration to 200–300 mg/L rendered the difference in reactivity less marked among the different composite resins. These findings suggest that the Cr(VI) removal rate of the composite resin with nZVI distributed in the periphery was relatively higher than that of the composite resin with a relatively uniform distribution of nZVI.

3.3.3. Effect of coexisting ions on Cr(VI) removal

Natural water contains many coexisting ions such as phosphate, nitrate, and silicate, which can interfere with the removal process. At 7 mg/L Cr(VI), the removal rates of the four composite resins were over 95%. Hence, the effect of phosphate, nitrate, and silicate coexisting ions on Cr(VI) removal for a Cr(VI) concentration of 7 mg/L was first investigated, as shown in Fig. 6. As the resin was a good adsorbent and anion exchanger, the concentration of coexisting ions was set as 100 mmol/L, which was more than 700 times the concentration of Cr(VI). In this experimental condition, the adsorption of the composite resins could be partially shielded, and the difference in the reductions of composite resins could be highlighted. It can be seen from Fig. 6 that nitrate had the greatest influence on the composite resins, followed by silicate and phosphate. As nitrate is a redox-sensitive anion, it could be reduced by nZVI to mainly NH_4^+ and a small amount of NO_2^- [27], thereby consuming a portion of nZVI in the process. Besides, previous studies have shown that a high concentration of anions could cause the passivation of ZVI, and that the passivation ability of nitrate was the strongest [28–30]. Therefore, nitrate has a greater inhibitory effect on the removal of Cr(VI). The addition of silica also inhibited the removal of Cr(VI), primarily because silicates could react with ZVI to form an outer complex and the reaction-generated oxidized ferric iron would react with silicates to form ferric hydroxide and silicic acid, which hindered further reaction [31,32]. The phosphate was found occupying the reactive surface sites of nZVI to form inner-sphere complexes [33]. This is also in line with the experimental results.

As seen from Fig. 6, D4 has a better removal performance than the others under the influence of these coexisting ions. The removal efficiency of D4 was 1.3 times that of D1 and the removal rate was 92% under the effect of phosphate, while the removal rate of D4 is 1.9 times that of D1 under the effect of nitrate. These results imply that the iron in D1 was mainly in the periphery, which was easily influenced by the coexisting ions, and the redox properties of nZVI were affected due to the influences of the coexisting ions, either by the formation of an oxide film or by the passivation of nZVI.

3.3.4. Cr(VI) removal kinetics by four nZVI nanocomposites

The kinetic adsorption behaviors of the four composite resins are shown in Fig. 7. The pseudo-first-order and pseudo-second-order models were applied to simulate the kinetic data (Figs. 7a and b) [34]:

$$\ln\left(Q_e - Q_t\right) = \ln Q_e - K_1 t \tag{1}$$

$$\frac{t}{Q_t} = \frac{1}{K_2 Q_e^2} + \frac{t}{Q_e} \tag{2}$$

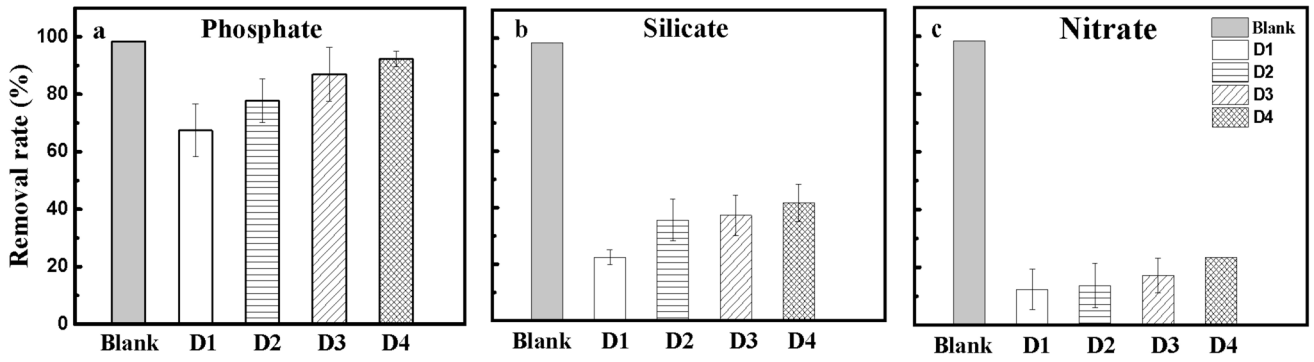

Fig. 6. Effects of coexisting ions on the Cr(VI) removal by D1-D4: (a) Phosphate, (b) Silicate and (c) Nitrate.

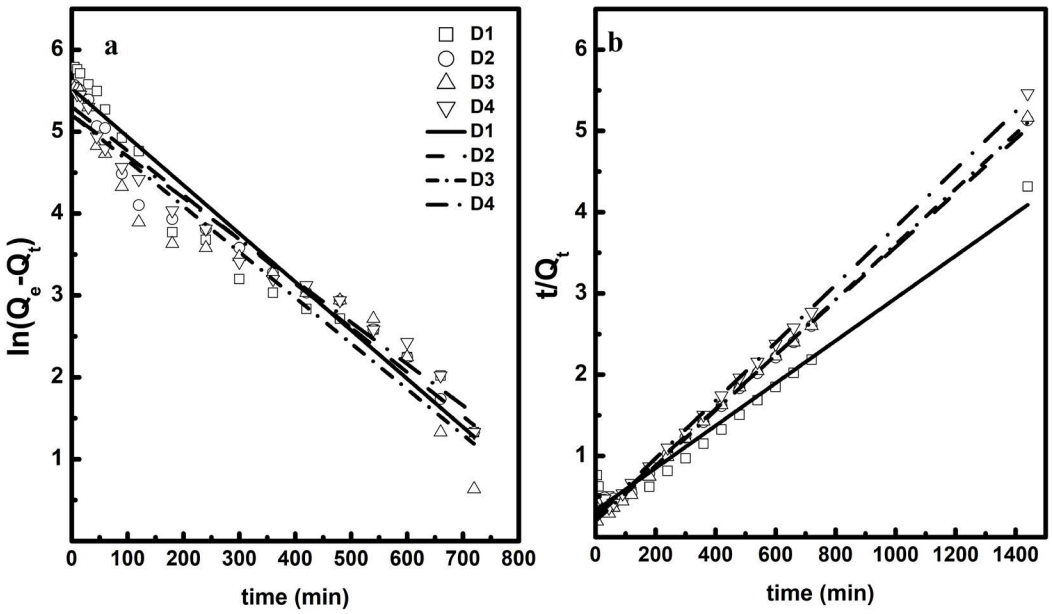

Fig. 7. Cr(VI) removal kinetics by four composite resins: (a) pseudo-first-order model and (b) pseudo-second-order model.

Q_e, K_1, and K_2 were calculated from the above formulae and the calculation results are shown in Table 1, where K_1 and K_2 represent the apparent first-order and observed second-order rate constants, respectively; Q_e and Q_t represent the equilibrium adsorption and real-time adsorption, respectively.

From the first-order and second-order kinetic fitting processes and the fitting parameters, it was found that the Cr(VI) removal process of the composite resin is in line with the second-order kinetics ($R^2 \geq 0.9710$). According to the second-order kinetics, Q_e and K_2 of the composite resins were 280.9–383.1 mg/g and 0.021–0.049 g/(mg min), respectively, when the initial concentration of Cr(VI) was 30 mg/L. In the results of Fu et al. [16], K_2 of the cation resin supported nZVI was 0.0013 g/(mg min), when the initial concentration of Cr(VI) was 30 mg/L. The kinetics of Cr(VI) removal was more rapid with the anion exchange resin stabilized nZVI compared with the cation exchange resin supported nZVI. According to published kinetic data [35], when the initial concentration of Cr(VI) was 10 mg/L, K_2 of Cr (VI) by nZVI was 0.0565 g/(mg min), which was significantly higher than that by composite resins. In general, the reaction rate of composite materials to target pollutants was lower than that of bare nZVI.

Fig. 7 shows that the reaction rate of D4 is higher among all the nanocomposites. However, the fitting parameters in Table 1 indicate that Q_e of D1 is the highest among four nanocomposites. Among the nanocomposites, K_2 of D1 was lower, but the removal amount was significantly higher. It can be seen that the distribution of zero-valent iron in the resin has significant effect on the entire removal process and the amount of removal.

3.4. Surface analysis of composite resins and removal mechanism

The above analyses showed that the nanocomposites with different Fe distributions had different reactivity under the same experimental condition. The removal of Cr(VI) by the composite resins involved three aspects: adsorption of resin, adsorption of nZVI, and reduction of nZVI [36,37]. The different removal activities might be related to the distribution of iron, which would affect the degree of these three

Table 1
Fitting parameters of kinetics

		Pseudo-first-order model			Pseudo-second-order model		
	$Q_{e,exp}$	Q_e	K_1	R^2	Q_e	K_2	R^2
	mg/g	mg/g	min^{-1}		mg/g	g/(mg min)	
D1	333.58	251.9	5.910	0.9492	383.1	0.021	0.9710
D2	280.65	201.7	5.410	0.9634	301.2	0.045	0.9966
D3	278.76	182.4	5.580	0.9249	294.1	0.058	0.9968
D4	263.64	182.7	5.070	0.9695	280.9	0.049	0.9975

aspects in the removal process. To understand the effect of nZVI distribution on the mechanism of Cr(VI) removal by the composite resins, the composite resins after the reaction were analyzed by XPS and the corresponding experimental results are shown in Fig. 8 and Table 2.

As shown in Fig. 8a, the Cr $2p_{3/2}$ XPS spectra of the composite resins after the reaction could be fitted into two peaks centered at 576.6 and 577.6 eV, which can be assigned to Cr(III) and Cr(VI), respectively [38]. A comparison of the four composite resins showed that the intensities of Cr(III) decreased from 80.5% to 44.5%, whereas the intensities of Cr(VI) increased from 19.5% to 55.5% from D1 to D4 (Fig. 8a and Table 2). This indicated that the reduction in D1 accounts for 75% of the total removal, while the reduction in D4 accounts for 50%. As shown in Fig. 8b, the Fe $2p_{3/2}$ XPS spectra of the composite resins after the reaction could be resolved into two peaks centered at 710.7 and 712.2 eV, which were assigned to Fe $2p_{3/2}$ of Fe(II) and Fe(III), respectively [39]. Table 2 showed that from D1 to D4, the intensities of Fe(II) decreased from 59.9% to 51.4%, while those of Fe(III) increased from 40.1% to 48.6%. The O 1s XPS spectra of the composite resins after the reaction (Fig. 8c) could be resolved into three peaks centered at 529.6, 531.2, and 532.6 eV, which can be assigned to structural oxygen (O^{2-}), hydroxyl (–OH), and adsorbed water (H_2O), respectively [40]. In addition, Table 2 shows that the percentage of hydroxides is higher. This indicated that most of the chromium was precipitated with the hydroxide of iron. Moreover, the structural oxygen in D1 was higher than that in the others.

The reduction and co-precipitation of Cr(VI) by ZVI occur through the following reactions [41,42]:

$$3Fe^0 + Cr_2O_7^{2-} + 7H_2O \rightarrow 3Fe^{2+} + 2Cr(OH)_3 + 8OH^- \quad (3)$$

Table 2
Composition of composite resins acquired by XPS

	Percentage composition (%)						
	Cr 2p		Fe 2p		O 1s		
	Cr^{3+}	Cr^{6+}	Fe^{2+}	Fe^{3+}	O^{2-}	OH^-	H_2O
D1	80.5	19.5	59.9	40.1	25.0	64.3	10.7
D2	50.5	49.5	53.6	46.4	23.2	67.0	9.9
D3	46.7	53.3	53.4	46.6	22.8	67.3	9.9
D4	44.5	55.5	51.4	48.6	18.1	72.4	9.6

$$6Fe^{2+} + Cr_2O_7^{2-} + 14H^+ \rightarrow 6Fe^{3+} + 2Cr^{3+} + 7H_2O \quad (4)$$

$$Fe^{2+} + 2Cr^{3+} + H_2O \rightarrow FeCr_2O_4 + 8H^+ \quad (5)$$

$$xCr^{3+} + (1-x)Fe^{3+} + 3H_2O \rightarrow (Cr_xFe_{1-x})(OH)_{3(s)} + 3H^+ \quad (6)$$

Fe^0 reacts with $Cr_2O_7^{2-}$ to form $Cr(OH)_3$ and Fe^{2+}. Fe^{2+} can transform to $Fe(OH)_2$ partially, following which $Fe(OH)_2$ is easily oxidized to $Fe(OH)_3$. Fe^{2+} could also react with $Cr_2O_7^{2-}$ to form Cr^{3+} and some Fe^{3+}. The formed Fe^{3+} can co-precipitate with Cr^{3+} in the aqueous solution. Fe^{2+} can also react with Cr^{3+} to form $FeCr_2O_4$ in the aqueous solution.

Among the four composite resins, D1 with a higher reducibility has more Cr(III), Fe(II), and O^{2-}, among the nanocomposites after the reaction. This illustrated that the nZVI in D1 most deoxidized Cr(VI) to Cr(III) and formed co-precipitates ($FeCr_2O_4$) with the Cr(III) oxidation form ($Cr_2O_4^{2-}$).

According to the above analysis, the Cr(VI) removal methods for the four composite resins had some differences: D1 had higher reducibility, and thus, most of the chromium reduced to trivalent chromium and precipitated out, while in D4, 44.5% chromium was reduced and 55.5% chromium was adsorbed or co-precipitated.

4. Conclusion

In this study, composite resins with different nZVI distributions were synthesized by adjusting the concentration of the reducing agent. The effect of nZVI different distributions on the performances (stability and reactivity) and removal mechanisms of the composite resins were investigated during Cr(VI) removal. The stability experiment showed that the loaded irons almost did not dissolve out at pH > 3, and that the iron in D4 was more firmly loaded. Further, pH and aging had no significant influences on the Cr(VI) removal rates of D1, D2, D3, and D4. The reactivity experiment showed that the Cr(VI) removal process of the composite resin was in line with the second-order kinetics, and that D1 had the highest removal capacity among the four nanocomposites (383.1 mg/g). Besides, phosphate, silicate, and nitrate could inhibit the chemical properties of the composite resins, and the degree of inhibition increased in the order of phosphate, silicate, and nitrate. Among the as-prepared composites with different nZVI distributions, the hybrids with a more uniform nZVI distribution exhibited a higher Cr(VI) removal efficiency for the same coexisting

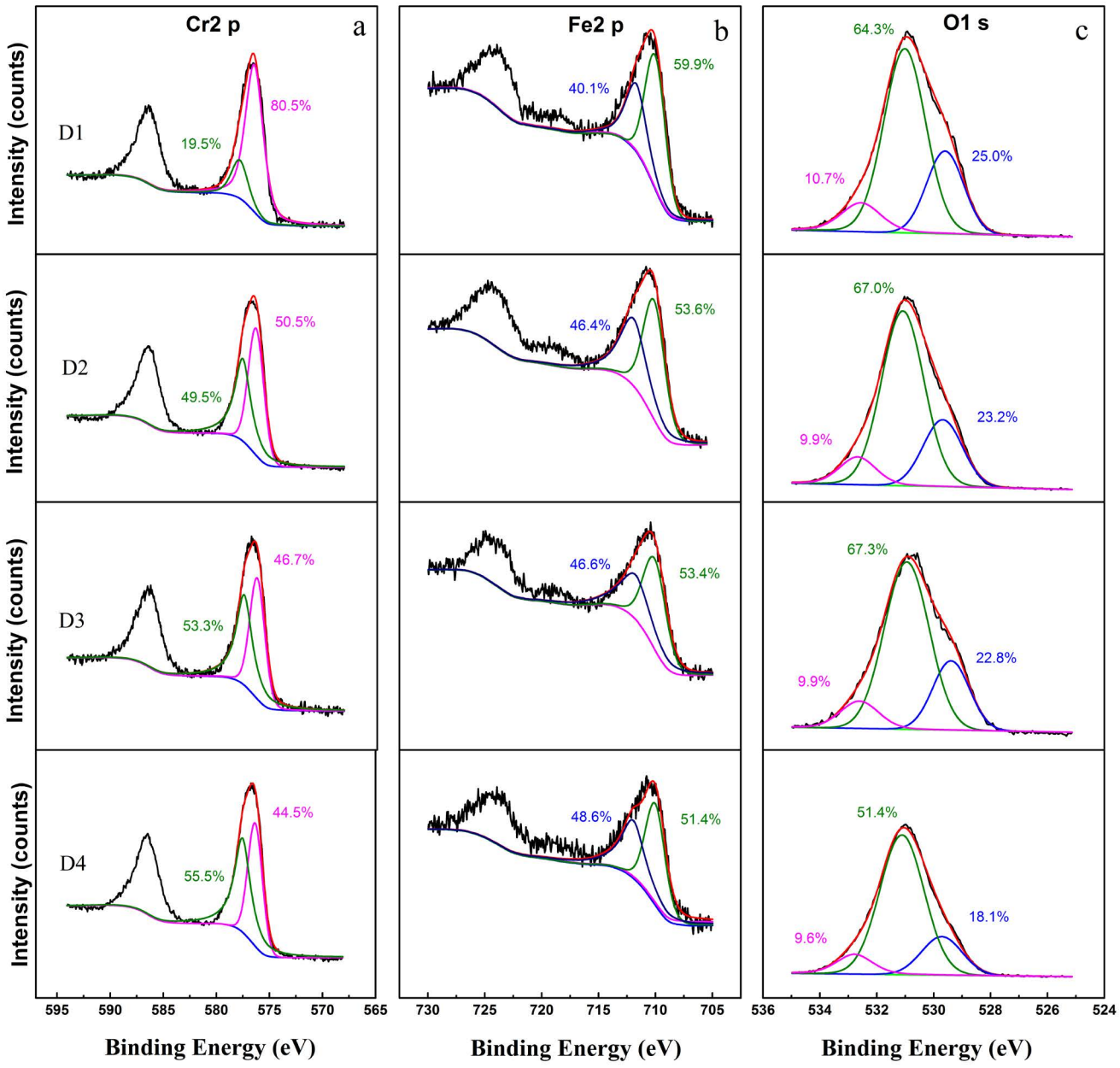

Fig. 8. XPS spectra of D1-D4 after reaction with Cr(VI): (a) Cr 2p, (b) Fe 2p and (c) O 1s.

ion. XPS analyses showed that the reducibility weakened while the adsorption or co-precipitation ability strengthened with increasing uniformity in the iron distribution. It might provide important insights into the relation between distribution of nZVI and the removal performance of the material, which could help in the design and development of nanomaterials for removing pollutants from water resources.

Acknowledgments

This work was supported by the National Natural Science Foundation of China (Grant Nos. 21707166 and 51608276), and the Natural Science Foundation of Jiangsu Province (Grant Nos. BK20160744 and BK20150978), and the Fundamental Research Funds for the Central Universities (No. 2632019ZD13), and the Cooperation Project of SEU-CPU (2242019K3DZ08).

References

[1] Y. Li, Z. Jin, T. Li, Z. Xiu, One-step synthesis and characterization of core-shell Fe@SiO_2 nanocomposite for Cr(VI) reduction, Sci. Total Environ., 421–422 (2012) 260–266.
[2] S. Sforzini, M.N. Moore, Z. Mou, M. Boeri, M. Banni, A. Viarengo, Mode of action of Cr(VI) in immunocytes of earthworms: implications for animal health, Ecotox. Environ. Saf., 138 (2017) 298–308.
[3] A. Ertani, A. Mietto, M. Borin, S. Nardi, Chromium in agricultural soils and crops: a review, Water Air Soil Pollut., 228 (2017) 190.

[4] G. Rojas, J. Silva, J.A. Flores, A. Rodriguez, M. Ly, H. Maldonado, Adsorption of chromium onto cross-linked chitosan, Sep. Purif. Technol., 44 (2005) 31–36.
[5] K.K. Krishnani, S. Ayyappan, Heavy metals remediation of water using plants and lignocellulosic agrowastes, Rev. Environ. Contam. Toxicol., 188 (2006) 59–84.
[6] P. Miretzky, A.F. Cirelli, Cr(VI) and Cr(III) removal from aqueous solution by raw and modified lignocellulosic materials: a review, J. Hazard. Mater., 180 (2010) 1–19.
[7] Y. Zou, X. Wang, A. Khan, P. Wang, Y. Liu, A. Alsaedi, T. Hayat, X. Wang, Environmental remediation and application of nanoscale zero-valent iron and its composites for the removal of heavy metal ions: a review, Environ. Sci. Technol., 50 (2016) 7290–7304.
[8] M. Stefaniuk, P. Oleszczuk, Y.S. Ok, Review on nano zerovalent iron (nZVI): from synthesis to environmental applications, Chem. Eng. J., 287 (2016) 618–632.
[9] X. Guan, Y. Sun, H. Qin, J. Li, I. Lo, D. He, H. Dong, The limitations of applying zero-valent iron technology in contaminants sequestration and the corresponding countermeasures: the development in zero-valent iron technology in the last two decades (1994–2014), Water Res., 75 (2015) 224–248.
[10] T. Tosco, M.P. Papini, C.C. Viggi, R. Sethi, Nanoscale zerovalent iron particles for groundwater remediation: a review, J. Cleaner Prod., 77 (2014) 10–21.
[11] L. Shi, Y. Lin, X. Zhang, Z. Chen, X. Zhang, Synthesis, characterization and kinetics of bentonite supported nZVI for the removal of Cr(VI) from aqueous solution, Chem. Eng. J., 171 (2011) 612–617.
[12] K. Xiong, Y. Gao, L. Zhou, X. Zhang, Zero-valent iron particles embedded on the mesoporous silica–carbon for chromium (VI) removal from aqueous solution, J. Nanopart. Res., 18 (2016) 267.
[13] C. Xu, L. Zhu, X. Wang, S. Lin, Y. Chen, Fast and highly efficient removal of chromate from aqueous solution using nanoscale zero-valent iron/activated carbon (NZVI/AC), Water Air Soil Pollut., 225 (2014) 1–13.
[14] P. Santander, D. Morales, B.L. Rivas, N. Kabay, I. Ipek, Ö. Kuşkum, M. Yuksel, M. Bryjak, Removal of Cr(VI) from aqueous solution by a highly efficient chelating resin, Polym. Bull., 74 (2017) 2033–2044.
[15] S.Wang, Y. Zhou, B. Gao, X. Wang, X. Yin, K. Feng, J. Wang, The sorptive and reductive capacities of biochar supported nanoscaled zero-valent iron (nZVI) in relation to its crystallite size, Chemosphere, 186 (2017) 495–500.
[16] F. Fu, J. Ma, L. Xie, B. Tang, W. Han, S. Lin, Chromium removal using resin supported nanoscale zero-valent iron, J. Environ. Manage., 128 (2013) 822–827.
[17] A. Toli, K. Chalastara, C. Mystrioti, A. Xenidis, N. Papassiopi, Incorporation of zero valent iron nanoparticles in the matrix of cationic resin beads for the remediation of Cr(VI) contaminated waters, Environ. Pollut., 214 (2016) 419–429.
[18] A. Toli, A. Varouxaki, C. Mystrioti, A. Xenidis, N. Papassiopi, Green Synthesis of resin supported nanoiron and evaluation of efficiency for the remediation of Cr(VI) contaminated groundwater by batch tests, Bull. Environ. Contam. Toxicol., 101 (2018) 711–717.
[19] Z. Jiang, S. Zhang, B. Pan, W. Wang, X. Wang, L. Lv, A fabrication strategy for nanosized zero valent iron (nZVI)-polymeric anion exchanger composites with tunable structure for nitrate reduction, J. Hazard. Mater., 233–234 (2012) 1–6.
[20] D. Gašparovičová, M. Králik, M. Hronec, A. Biffis, M. Zecca, B. Corain, Reduction of nitrates dissolved in water over palladium-copper catalysts supported on a strong cationic resin, J. Mol. Catal. A-Chem., 244 (1983) 258–266.
[21] Y. Xie, S. Zhang, B. Pan, L. Lv, W. Zhang, Effect of CdS distribution on the photocatalytic performance of resin-CdS nanocomposites, Chem. Eng. J., 174 (2011) 351–356.
[22] Q. Du, S. Zhang, B. Pan, L. Lv, W. Zhang, Q. Zhang, Effect of spatial distribution and aging of ZVI on the reactivity of resin–ZVI composites for arsenite removal, J. Mater. Sci., 49 (2014) 7073–7079.
[23] Q. Du, L. Zhou, S. Zhang, B. Pan, L. Lv, W. Zhang, Q. Zhang, Iron-mediated oxidation of arsenic(III) by oxygen and hydrogen peroxide: dispersed versus resin-supported zero-valent iron, J. Colloid Interface Sci., 428 (2014) 179–184.
[24] Editorial Board of Water and Wastewater Monitoring and Analysis Method of China Environmental Protection Administration, Water and Wastewater Monitoring and Analysis Method, 4th ed., China Environmental Science Press, China, 2002.
[25] Y. Sun, X. Li, W. Zhang, H. Wang, A method for the preparation of stable dispersion of zero-valent iron nanoparticles, Colloid Surf. A-Physicochem. Eng. Asp., 308 (2007) 60–66.
[26] Y. Sun, X. Li, J. Cao, W. Zhang, H.P. Wang, Characterization of zero-valent iron nanoparticles, Adv. Colloid Interface Sci., 120 (2006) 47–56.
[27] B.A. Till, L.J. Weathers, P.J.J. Alvarez, Fe(0)-supported autotrophic denitrification, Environ. Sci. Technol., 32 (1998) 634–639.
[28] R.M. Cornell, U. Schwertmann, The iron oxides: structure, properties, reactions, occurrence and uses, Mineral. Mag., 61 (1997) 740–741.
[29] Y. Liu, T. Phenrat, G.V. Lowry, Effect of TCE concentration and dissolved groundwater solutes on NZVI-promoted TCE dechlorination and H_2 evolution, Environ. Sci. Technol., 41 (2007) 7881.
[30] B.C. Reinsch, B. Forsberg, R.L. Penn, C. Kim, G.V. Lowry, Chemical transformations during aging of zerovalent iron nanoparticles in the presence of common groundwater dissolved constituents, Environ. Sci. Technol., 44 (2010) 3455.
[31] C. Le, J.H. Wu, S.B. Deng, P. Li, X.D. Wang, N. Zhu, P. Wu, Effects of common dissolved anions on the reduction of parachloronitrobenzene by zero-valent iron in groundwater, Water Sci. Technol., 63 (2011) 1485–1490.
[32] T. Kohn, A.L. Roberts, The effect of silica on the degradation of organohalides in granular iron columns, J. Contam. Hydrol., 83 (2006) 70–88.
[33] C. Su, R. Puls, Nitrate reduction by zerovalent iron: effects of formate, oxalate, citrate, chloride, sulfate, borate, and phosphate, Environ. Sci. Technol., 38 (2004) 2715–2720.
[34] B. Song, P. Xu, G. Zeng, J. Gong, X. Wang, J. Yan, S. Wang, P. Zhang, W. Cao, S. Ye, Modeling the transport of sodium dodecyl benzene sulfonate in riverine sediment in the presence of multi-walled carbon nanotubes, Water Res., 129 (2018) 20–28.
[35] S.S. Poguberović, D.M. Krcmar, S.P. Maletić, Z. Kónya, D. Tomasevic, D.V. Kerkez, S.D. Rončević, Removal of As(III) and Cr(VI) from aqueous solutions using "green" zero-valent iron nanoparticles produced by oak, mulberry and cherry leaf extracts, Ecol. Eng., 90 (2016) 42–49.
[36] X. Lv, Y. Hu, J. Tang, T. Sheng, G. Jiang, X. Xu, Effects of co-existing ions and natural organic matter on removal of chromium (VI) from aqueous solution by nanoscale zero valent iron (nZVI)-Fe_3O_4 nanocomposites, Chem. Eng. J., 218 (2013) 55–64.
[37] D. Chang, T. Chen, H. Liu, Y. Xi, C. Qing, Q. Xie, R.L. Frostc, A new approach to prepare ZVI and its application in removal of Cr(VI) from aqueous solution, Chem. Eng. J., 244 (2014) 264–272.
[38] R. Fu, X. Zhang, Z. Xu, X. Guo, D. Bi, W. Zhang, Fast and highly efficient removal of chromium (VI) using humus-supported nanoscale zero-valent iron: Influencing factors, kinetics and mechanism, Sep. Purif. Technol., 174 (2017) 362–371.
[39] L. Xu, J. Wang, Magnetic nanoscaled Fe_3O_4/CeO_2 composite as an efficient Fenton-like heterogeneous catalyst for degradation of 4-chlorophenol, Environ. Sci. Technol., 46 (2017) 10145–10153.
[40] N. Sleiman, V. Deluchat, M. Wazne, M. Mallet, A. Courtin-Nomade, V. Kazpard, M. Baudu, A. Courtin-Nomade, V. Kazpard, Phosphate removal from aqueous solution using ZVI/sand bed reactor: behavior and mechanism, Water Res., 99 (2016) 56–65.
[41] Z. Fang, X. Qiu, R. Huang, X. Qiu, M. Li, Removal of chromium in electroplating wastewater by nanoscale zero-valent metal with synergistic effect of reduction and immobilization, Desalination, 280 (2011) 224–231.
[42] K. Nagata, R. Nishiwak, Y. Nakamura, T. Maruyama, Kinetic mechanisms of the formations of $MgCr_2O_4$ and $FeCr_2O_4$ spinels from their metal oxides, Solid State Ion., 49 (1991) 161–166.